

This is the accepted manuscript made available via CHORUS. The article has been published as:

# Kinetics of Domain Switching by Mechanical and Electrical Stimulation in Relaxor-Based Ferroelectrics

Zibin Chen, Liang Hong, Feifei Wang, Xianghai An, Xiaolin Wang, Simon Ringer, Long-Qing Chen, Haosu Luo, and Xiaozhou Liao

Phys. Rev. Applied **8**, 064005 — Published 6 December 2017

DOI: [10.1103/PhysRevApplied.8.064005](https://doi.org/10.1103/PhysRevApplied.8.064005)

# **The Kinetics of Domain Switching in Relaxor-Based Ferroelectrics by Mechanical and Electrical Stimulation**

Zibin Chen<sup>1†</sup>, Liang Hong<sup>2†</sup>, Feifei Wang<sup>3</sup>, Xianghai An<sup>1</sup>, Xiaolin Wang<sup>4</sup>, Simon Ringer<sup>1,5</sup>,

Long-Qing Chen<sup>2</sup>, Haosu Luo<sup>6</sup>, Xiaozhou Liao<sup>1\*</sup>

\* Correspondence and requests for materials should be addressed to [Xiaozhou.liao@sydney.edu.au](mailto:Xiaozhou.liao@sydney.edu.au)

† These authors contributed equally to this work.

<sup>1</sup> School of Aerospace, Mechanical and Mechatronic Engineering, The University of Sydney, Sydney, NSW  
2006, Australia,

<sup>2</sup> Department of Materials Science and Engineering, Pennsylvania State University, University Park,  
Pennsylvania 16802, USA,

<sup>3</sup> Key Laboratory of Optoelectronic Material and Device, Department of Physics, Shanghai Normal University,  
Shanghai 200234, China,

<sup>4</sup> Institute for Superconducting and Electronic Materials, Faculty of Engineering, Australian Institute for  
Innovative Materials, University of Wollongong, NSW 2522, Australia,

<sup>5</sup> Australian Institute for Nanoscale Science and Technology, The University of Sydney, NSW, 2006, Australia,

<sup>6</sup> Key Laboratory of Inorganic Functional Materials and Devices, Shanghai Institute of Ceramics, Chinese  
Academy of Sciences, Shanghai 200050, China.

## Abstract

Ferroelectric materials have been extensively explored for applications in high-density non-volatile memory devices because of their ferroelectric/ferroelastic domain switching behaviour under electric loading or mechanical stress. However, the existence of ferroelectric and ferroelastic backswitching would cause significant data loss, which affects the reliability of data storage. Here we applied in-situ transmission electron microscopy and phase-field modelling to explore the unique ferroelastic domain switching kinetics and the origin of this in relaxor-based  $\text{Pb}(\text{Mg}_{1/3}\text{Nb}_{2/3})\text{O}_3$ -33% $\text{PbTiO}_3$  single crystal pillars under electrical and mechanical stimulations. Results showed that the electric/mechanical hysteresis loop shifted for relaxor-based single crystal pillars because of the low energy levels of domains in the material and the constraint on the pillars, resulting in various mechanically reversible and irreversible domain switching states. The phenomena can potentially be used for advanced bit writing and reading in non-volatile memories, which effectively overcomes the backswitching problem and broadens the types of ferroelectric materials for non-volatile memory applications.

## 1. Introduction

Ferroelectric materials exhibit intrinsic coupling of spontaneous polarization and strain. Their ferroelectric/ferroelastic domains can be reversibly switched with voltage bias or mechanical stress. This characteristic has been used for high-density non-volatile memories[1-6]. In these devices, two opposite polarization directions act as the two logical signals, serving as memory bits which can be written and read through applying electric field.[3,7] However, the instability of written ferroelectric domains, e.g., the time-dependent ferroelectric backswitching, has been a long-standing problem that causes significant data loss.[8-12] Such backswitching results from the surface electrostatic or internal build-in elastic energy[8,13,14] and has higher impact on domains with small sizes. Small domain sizes are critical for high-density storage.[15] However, the relaxation of high-energy domain walls drives significantly ferroelectric backswitching when switched domain sizes are small.[8] Recently, ferroelastic domain switching by electrical stimulus has also been considered for memory applications.[16,17] However, the high elastic strain energy accompanying the ferroelastic domain switching tends to relax the switched domains, causing ferroelastic backswitching at zero bias.[16,18] Both ferroelectric and ferroelastic backswitching suggests the lack of reliability in domain switching under electrical stimulus. Mechanical excitation is another possible way for controlling ferroelectric/ferroelastic domain switching.[5,19,20] Mechanical writing of ferroelectric polarization in a BaTiO<sub>3</sub> film has been realized, [5] in which polarization is 180° reversed by mechanical loading as a result of a large strain gradient applied to the film surface by a probe via the mechanism of flexoelectricity.[21,22] Although stable domain patterns without relaxation for days are generated by mechanical writing, written domains are not reversible because of the unidirectional nature of the mechanical loading. Therefore, a new approach to overcome the abovementioned limitations of using

either electrical or mechanical excitation for memory applications of ferroelectric materials is necessary.

Relaxor-based ferroelectric single crystals with chemical compositions in the vicinity of the morphotropic phase boundary (MPB) have recently attracted significant attention due to their unique hysteresis behaviour, ultrahigh piezo-electric properties and electromechanical coupling factors.[23] Compared with normal ferroelectrics, relaxor-based ferroelectrics in MPB have abnormally small domain wall energies, small coercive fields, [24] and miniature domain sizes which allow easy redistribution of invariant domain populations.[25] The domain switching kinetics in relaxor-based ferroelectric is different from that in normal ferroelectrics, which leads to the possibility of overcoming the above-mentioned drawback. Previous researches focused on the macroscopic materials responses of relaxor-based ferroelectric materials to electric or mechanical loading,[23,26,27] little has been known on their microscopic responses.

Here we applied in-situ transmission electron microscopy (TEM) [25,28,29] and phase-field modelling [30] to explore the ferroelastic domain switching kinetics under applied electrical and/or mechanical stimuli in  $\text{Pb}(\text{Mg}_{1/3}\text{Nb}_{2/3})\text{O}_3$ -33% $\text{PbTiO}_3$  (PMN-33%PT) relaxor-based single crystals. It was found that ferroelastic domain structures in PMN-33%PT single crystals are fully recoverable under a mechanical loading–unloading cycle (the mechanically-reversible state) before electrical biasing. After applying a bias, domains become sensitive to mechanical load and exhibit only partial recovery (the mechanically-irreversible state). However, the mechanically-irreversible state returns to the mechanically-reversible state after another mechanical loading-unloading cycle. Our results present the fundamental physics of domain switching behaviour in relaxor-based ferroelectrics and provide an approach to recover ferroelastic domain structures via a successive cycling of mechanical and electrical stimuli. Based on these discoveries, instead of trying to overcome

the intrinsic instability of written ferroelectric domains, we propose a conceptual strategy to take advantage of the mechanically-irreversible state and the mechanically-reversible state for reliable bit writing and reading in non-volatile memory devices. This expands the number of potential candidate materials for non-volatile memory devices.

## 2. In-situ experiment and phase-field simulations

**Figure 1a** presents a schematic of the in-situ experimental setup. A bulk PMN-33%PT was fixed on a Cu plate using Pt deposition. Multiple PMN-33%PT pillars with dimensions of  $2.0\ \mu\text{m} \times 1.6\ \mu\text{m} \times 0.06\ \mu\text{m}$  (length  $\times$  width  $\times$  thickness) were produced using mechanical grinding and focused ion-beam (FIB) processing. In-situ mechanical and electrical stimulations in TEM were applied by a conductive tip. The Cu plate acted as an electrode and the conductive tip as the other electrode. A typical domain configuration observed from a pillar is presented in Figure 1b. Two types of domains appeared with different contrast.

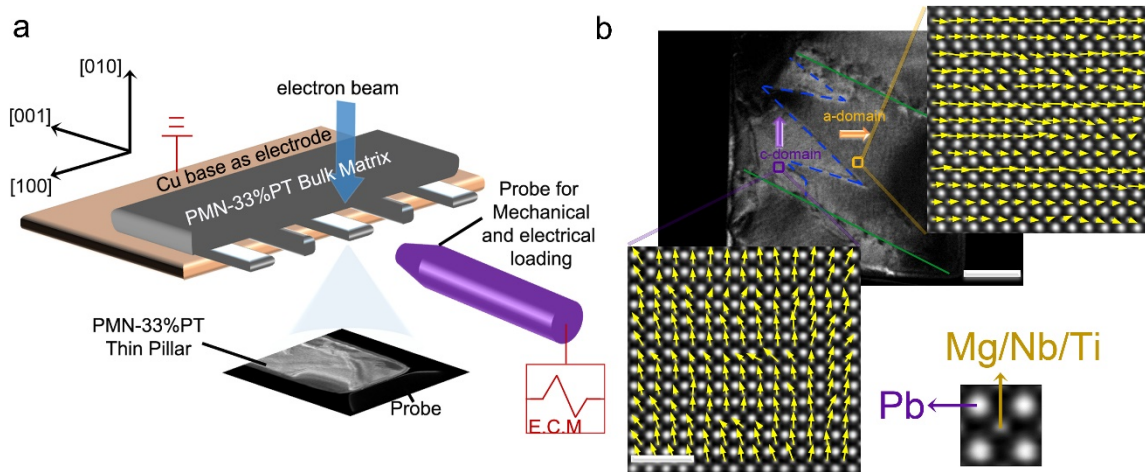
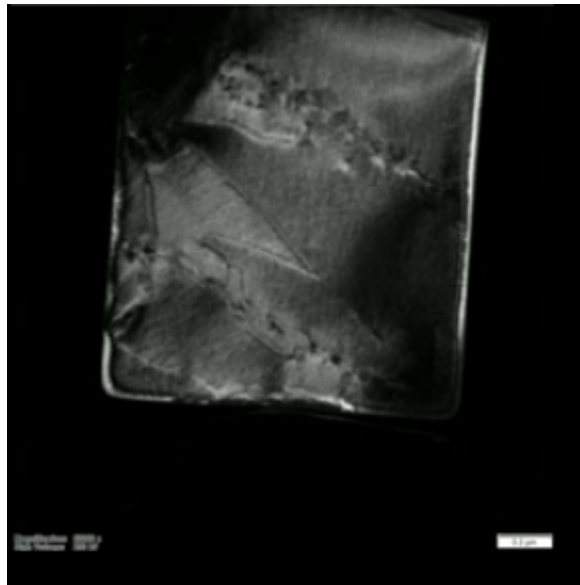


**Figure 1.** In situ TEM set-up and ferroelastic domain configurations. **(a)** Schematic diagram of experimental set-up. A bulk PMN-33%PT matrix with thin pillars was fixed on a grounded Cu platform using Pt deposition. A conductive tip connected to the Electrical Characterization Module (E.C.M.) acts as an indenter and electro for mechanical and electrical loading. The actual allocation of the pillar and the tip was captured in the enlarge TEM image. **(b)** Dark-field TEM image (Scale bar, 400 nm) and STEM-HAADF images (Scale bar, 1 nm) showing a head-to-tail tetragonal a/c-domain configuration. Domain walls are indicated using blue dash lines. Two parallel green lines indicate the area investigated in this study.

PMN-xPT with the composition  $x=33\%$  is at MPB having a monoclinic structure.[31,32] The ferroelectric adaptive phase theory[33-35] suggests that monoclinic phases, consisting of miniaturization of stress-accommodating tetragonal domains, are microdomain-averaged of tetragonal phases. A moderate constraint on the pillar exerted by the existence of oxygen vacancy, topological defects and/or compositional variation in the relaxor-bases single crystal is thus prone to a head-to-tail  $90^\circ$  ferroelastic domain configuration.[36-38] This is confirmed by atomic-resolution scanning TEM (STEM) high-angle annular dark-field (HAADF) images shown in Figure 1b. Through the measurement of the displacement between Pb cations and their surrounding Mg/Nb/Ti cations in the HAADF images,[39,40] domains with light contrast (the c-domain) are determined to have their polarization upward (see the bottom-left HAADF image) and domains with dark contrast (the a-domain) have their polarization pointing to the right (see the top-right HAADF image), indicating that neighbouring domains have a head-to-tail  $90^\circ$  domain relationship. The  $90^\circ$  domain boundaries in Figure 1b are indicated using blue dash lines. Two parallel green lines were drawn in Figure 1b to indicate the area of focus for the following investigation of domain switching phenomena induced by external stimulation.

Stress was applied to pillars through moving the flat conductive tip toward the pillars in the displacement control mode with the displacement rate of 3nm/s for approaching and -4nm/s for retraction. The evolution of domain configuration during a mechanical loading-unloading cycle and the related load/bias–time curves (bias = 0) are shown in **Figure 2a** (extracted from the **Movie 1** in the supplementary information [41-56]) and 2b, respectively. Points 1 (before loading), 2, 3, and 4 in Figure 2b correspond to the first, second, third, and fourth domain configuration in Figure 2a, respectively. With increasing load, the c-domain shrank and the a-domain expanded through the motion of the  $90^\circ$  domain boundaries toward the c-domain. The initiation of the domain switching started from domain boundaries. When

the applied load reached 22  $\mu\text{N}$ , the whole area was mostly occupied by a single a-domain. Upon unloading, the domain configuration evolved in the opposite direction and the original domain configuration was fully recovered. The dark contrast lines in c-domain shown in figure 2a (indicated by arrows) exists widely in relaxor-based ferroelectrics. It is caused by the existence of nano polar regions[57] or regions of dipole glass in relaxor-based ferroelectrics [58-60]. These regions have local polarization variation compared with their surrounding areas. Because the loading and unloading processes were displacement control with constant displacement rates, the approximate linear load–time curve for approaching and retraction and the inset fully reversible load-displacement curve in Figure 2b indicate that the deformation process of the pillar was elastic without noticeable bending.



**Movie 1.** A mechanical loading-unloading cycle

The maximum load was always kept to  $\sim 28 \mu\text{N}$  to make sure the comparability of different loading/unloading experiments. The maximum load corresponds to an applied stress of  $\sim 300 \text{ MPa}$ , which is very small compared to the fracture strength of the material and therefore did not damage the material.[61,62] The applied stress needed to initiate domain wall motion in this sample was around  $40 \text{ MPa}$ , which is well below the values reported for



other materials.[61] This type of domain wall motion is easily triggered due to the unpinning effect to the domain walls, which are commonly observed in relaxors around MPB.[63,64]

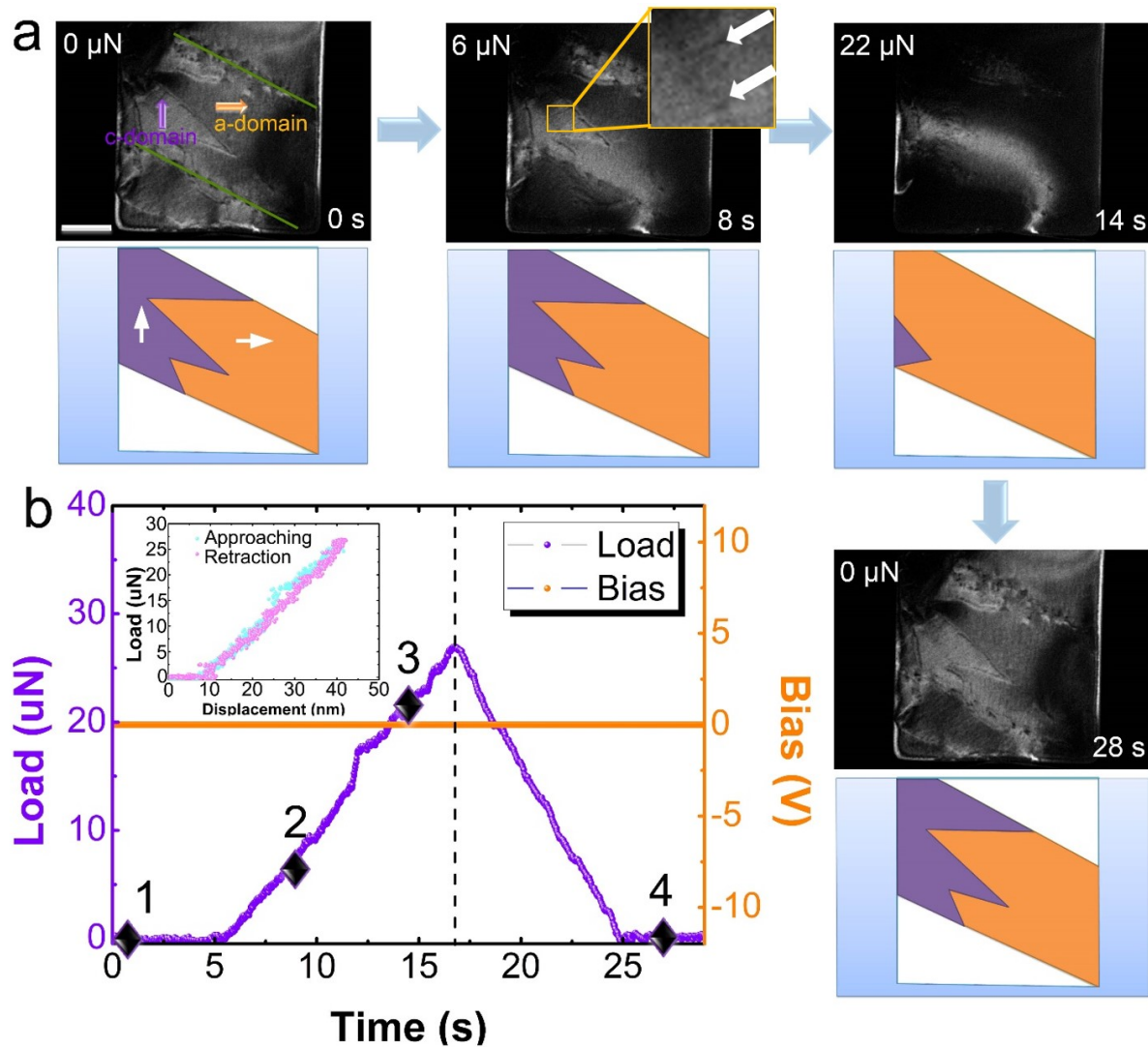


**Figure 2.** Ferroelastic domains switching by mechanical excitation. (a) A series of images (extracted from the Movie 1 in the supplementary information) showing the evolution of ferroelastic domains under mechanical excitation. Domains were fully reversed after a mechanical loading-unloading cycle. Scale bar, 400 nm. (b) A load/bias-time curve showing the real-time application of mechanical load with zero bias. Numbers 1 to 4 correspond to the image order in (a), indicating the position of the images in the curve. A load-displacement curve is shown in the inset graph.

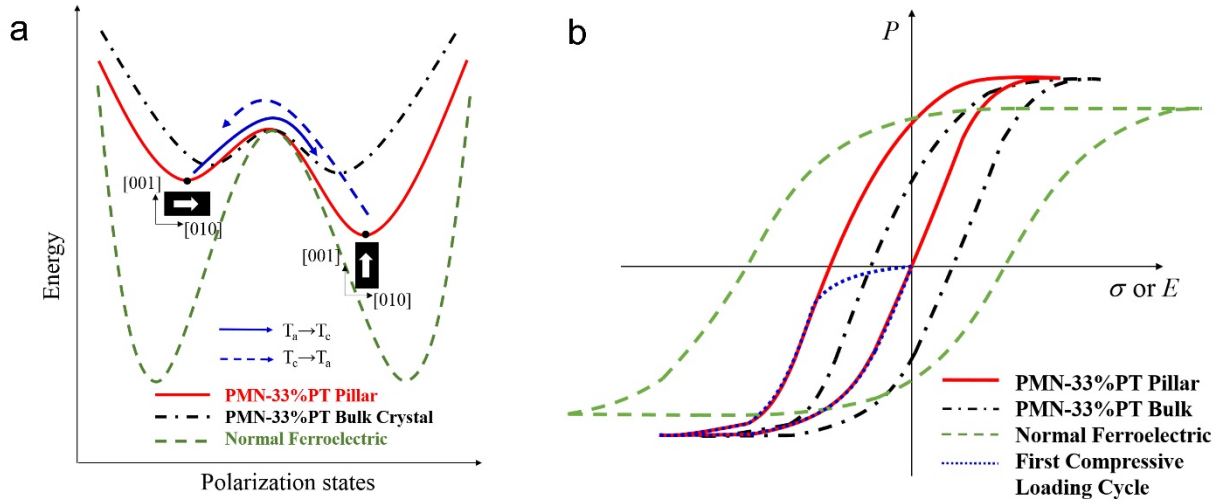


**Figure 3.** Domain switching kinetics in a single-crystal PMN-33%PT pillar predicted by phase-field calculations. (a) The asymmetric energy barrier between a- and c- tetragonal ferroelastic domains (red solid line). Mechanical constraint exerted to the pillar breaks the original symmetric energy barrier, resulting in an easier domain transition from a-domain to c-domain (blue solid vector) compared to the reverse transition path (blue dash vector). Such different transition paths is not obvious in normal ferroelectrics due to their large energy barriers. (b) A displaced hysteresis loop (red solid line) for the PMN-33%PT pillar. Also displayed are hysteresis loops of a bulk relaxor single crystal (black dash line) and normal ferroelectrics (green dash line).

To explain the observed phenomenon in Figure 2, phase-field calculations were conducted and the results are shown in **Figure 3**. In our previous research[20], we demonstrated that domain switching in PMN-38%PT occurs via the nucleation and growth of nanodomains because of the much smaller energy of nanodomains than bulk domains in PMN-38%PT. It is also reported that the strong pinning force acts on the domain walls, leading to nano-domain nucleation and motion rather than bulk domain wall motion in this material.[20] In contrast, domain switching in PMN-33%PT reported here occurs via bulk domain motion, which is caused by the low energy of bulk domains in PMN-33%PT and lack of pinning force on the domain walls. For the PMN-33%PT with a unit-cell volume of  $64.9 \text{ \AA}^3$  at room temperature, phase-field calculations showed that the energy of a single tetragonal a- and c-domain (see details in the phase-field calculations in the Supplementary Information S3) in a pillar is  $-0.443 \text{ meV}$  and  $-1.05 \text{ meV}$ , respectively, which is smaller than the energy of

domains in PMN-38%PT and is two orders of magnitude smaller than the energy ( $\sim 100$  meV) of tetragonal domains in normal ferroelectric materials. Notice that the energy of a domain or a domain structure represents the difference in energies between the cubic state and the tetragonal state (including a-domain and c-domain). The calculated energy of the bulk single tetragonal domain includes ferroelastic energy and bulk free energy. The smaller energy of  $90^\circ$  domain structure in PMN-33%PT without strong pinning effect on domain walls indicated that the nucleation of nanodomain in PMN-33%PT is not energetically necessary and bulk domain wall motion is preferred. The reversible domain switching in a mechanical loading-unloading cycle results from two reasons: (1) a small external field can activate domain wall motion due to the small energy barrier among tetragonal domains.[24] This agrees with the easy polarization rotation around MPB; and (2) the elastic constraint to the PMN-33%PT pillar leads to remarkably different stress states for in-plane a-domains and out-of-plane c-domains, resulting in an asymmetric energy barrier between the two domains. In particular, the domain transition from a-domain to c-domain has a lower energy barrier (red solid line) as shown in Figure 3a. Figure 3b shows the hysteresis loops of normal ferroelectrics (the green dash line), bulk PMN-33%PT (the black dash line), and PMN-33%PT pillars (the red solid line). Compared to the hysteresis loop of normal ferroelectrics, the hysteresis of a bulk PMN-33%PT single crystal is slim with a small coercive field.[23] An asymmetric and low energy barrier of the PMN-33%PT pillar displaces the slim hysteresis to the left, making the initial ferroelastic domain structure closer to the domain state at a positive coercive field as shown in Figure 3b. As a result, a compressive loading-unloading cycle (blue dash line in Figure 3b) can recover the initial ferroelastic domain structure. Figure 3b also indicates an irreversible state of polarization when a positive bias or a tension loading is applied (red solid line). This irreversible state can be compensated by applying a negative bias or a compression stress, leading to the recovery of the initial state.

Such reversible hysteresis loops were observed in a  $\langle 001 \rangle$  poled  $\text{Pb}(\text{Zn}_{1/3}\text{Nb}_{2/3})\text{O}_3$ - $\text{PbTiO}_3$  relaxor-based single crystal with the easily activated  $71^\circ$  domain rotation.[23] In an aged  $\text{BaTiO}_3$  single crystal, a defect-induced internal field pins and retracts ferroelastic domain wall motion, leading to reversible domain switching.[65] However, these two reversible phase transition processes were studied based on macro-scale observations without knowing the effects of complex domain structures and heterogeneous nucleation of new domains. The present study, which utilized the asymmetric domain transition kinetics between tetragonal a- and c-domains in the ubiquitous microscopic  $90^\circ$  head-to-tail ferroelastic domain configuration, demonstrated a new approach for reversible domain switching.

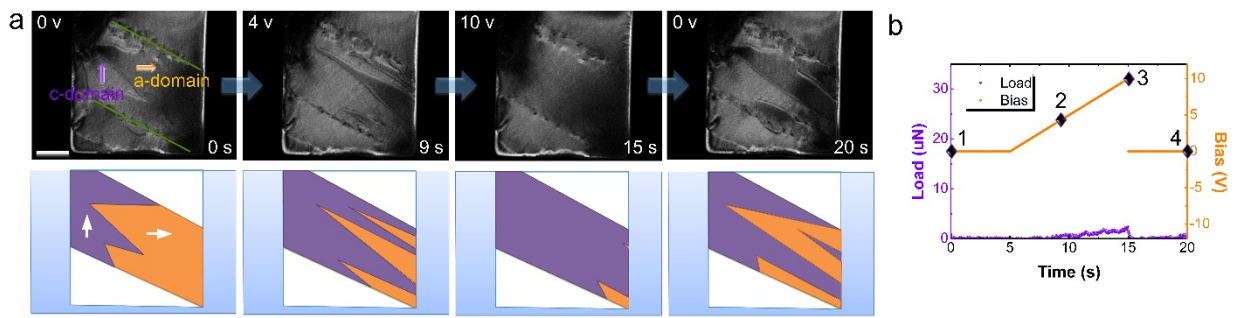
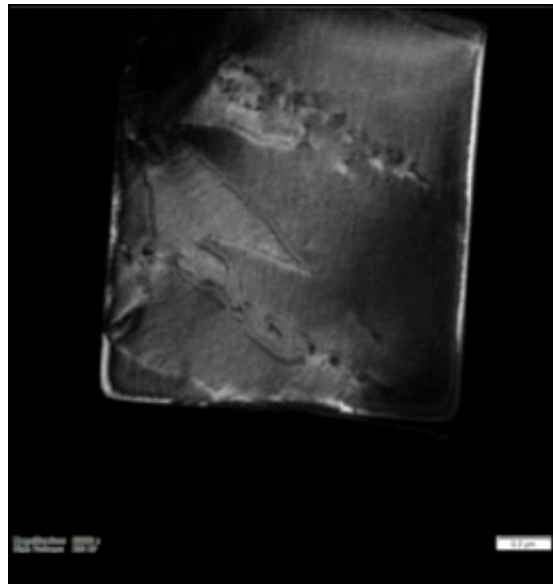


**Figure 4.** Ferroelastic domains switching by electrical excitation. **(a)** A series of images (extracted from the Movie 2 in the supplementary information) showing the evolution of ferroelastic domains under electrical loading. Scale bar, 400nm. **(b)** A load/bias–time curve. No mechanical load was applied during the whole process. The bias was applied from 0V (5 s) to +10V (15 s) with the ramping rate of 1V/s.

The effect of a voltage bias on domain configuration is presented in **Figure 4a** (extracted from the **Movie 2** in the supplementary information). The corresponding load/bias–time curve (external load = 0) is illustrated in Figure 4b. Again, points 1, 2, 3, and 4 in Figure 4b correspond to the first, second, third, and fourth image in Figure 4a. Gentle contact between the conductive tip and the pillar was held for the close-loop electrical loading experiment. The bias was raised from 0V to +10V between 5 s and 15 s with the

ramping rate of 1V/s as shown in Figure 4b. Although no mechanical load was applied, there was still small load detected, which was caused by the electrostrictive effect[66] in ferroelectric materials. With the increase of the bias from 0V to +2V (5 s to 7 s in the Movie 2 in the supplementary information), the domain configuration did not change as the initiation energy for domain motion was not reached. Further increasing the bias resulted in the shrinkage of the a-domain and the simultaneous expansion of the c-domain. When the bias was increased to +10V, the whole area was occupied by nearly a single c-domain as shown in the third image in Figure 4a. After retraction of the bias at 15 s, the a-domain back-switched and was gradually stabilized at 20 s as shown in Figure 4a. Comparison of the initial and final domain configurations shows that the area of the c-domain increased after an electrical loading cycle, i.e., the domain configuration was only partially recovered. This is consistent to our proposed mechanism indicated in Figure 3b. The resulting domain structure was stable and remain unchanged after 4 weeks.



**Movie 2.** An electrical loading-unloading cycle

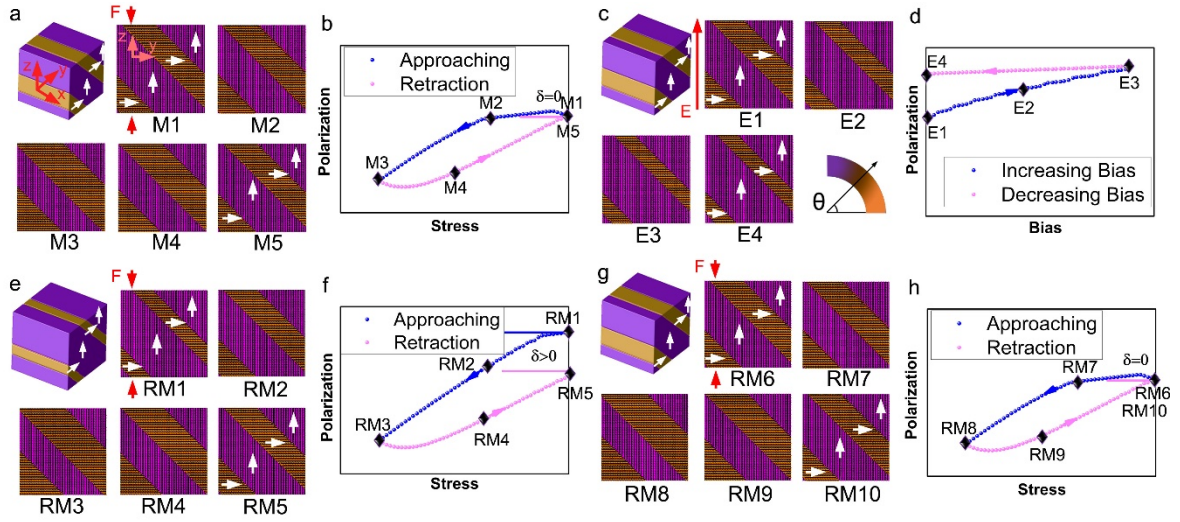


**Figure 5.** Phase-field modelling (a, c, e, g) ferroelastic domain switching under a mechanical loading cycle, an electrical loading cycle, a mechanical loading cycle after electric loading, and a mechanical loading cycle after previous mechanical loading, respectively. White arrows represent the directions of polarization. (b, d, f, h) Closed and open polarization–load curves corresponding to the phase-field modelling in a, c, e, and g, respectively. The blue lines indicate the loading process and the pink lines the unloading process.

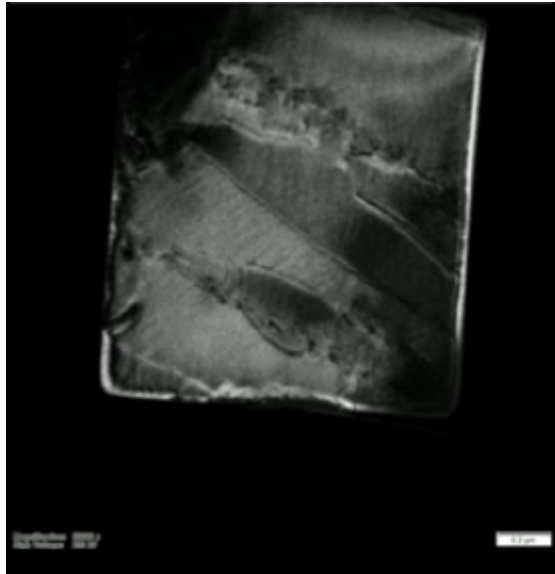
Phase-field modelling shown in **Figure 5** confirms the experimental results. It suggested a stable domain configuration in a tetragonal ferroelectric holds  $90^\circ$  ferroelastic domain walls, which move along the direction normal to domain wall planes under mechanical loading, as shown in Figure 5a. Polarization rotation occurs only around the domain walls.[67] One interesting feature of this initial ferroelastic domain configuration in the PMN-33%PT pillar is that this domain state locates around the positive coercive field. When a compressive loading-unloading cycle is applied, phase-field modelling suggested a recoverable domain switching as shown in Figure 5a and 5b. The change of polarization state  $\delta$  before and after this mechanical cycle is zero. Figure 5b shows a nucleation regime that activates the domain transition from c-domain to a-domain exists at the beginning of the compressive loading process (the increase of polarization region). After the domain wall motion is activated, the polarization varies monotonically with the external stimulus, which resulted from the soft pinning force to domain wall motion in the PMN-33%PT pillar. When positive voltage bias is applied to the initial ferroelastic domain structure, an incubation stage

for domain wall motion to promote the transition from a-domain to c-domain is not obvious (Figure 5c and 5d). In the bias unloading process, however, the energy released by the electric unloading process is not sufficient to activate reverse domain wall motion, pinning the domain wall motion. Thus, the domain structure does not reverse in this electrical loading-unloading cycle as shown in Figure 5c and Figure 5d.

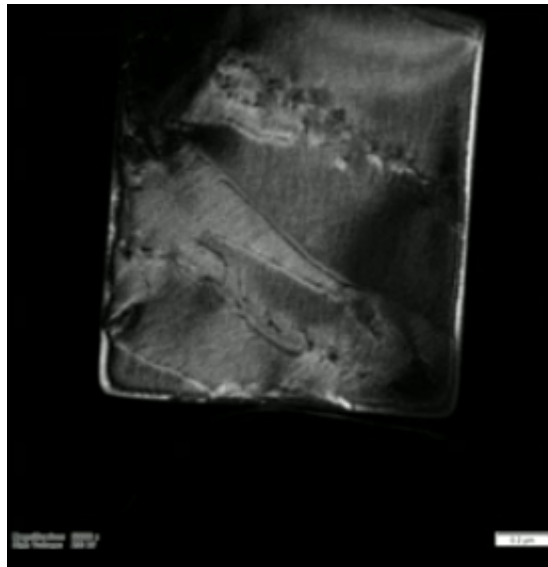
Interestingly, mechanical loading after an electrical loading cycle erased the polarization introduced by the electrical loading–unloading cycle (Figure 5e). In consistence to Figure 3b, the original ferroelastic domain configuration was recovered by applying a mechanical loading-unloading cycle. As a result, the stress-polarization loop is not a closed one (Figure 5f), i.e., the change of polarization  $\delta$  is not zero. After the first mechanical loading-unloading cycle following electrical cycles, the second mechanical loading-unloading cycle was applied, leading to reversible domain switching in Figure 5g and 5h. The phase-field simulation results were consistent to the proposed domain switching kinetics shown in Figure 3b.

Experiments were conducted to confirm the phase-field simulation results on mechanical loading-unloading cycles after an electrical loading cycle. After an electrical loading cycle, mechanical loading–unloading cycles were applied to the same area as shown in **Figure 6** and **Movie 3** and **Movie 4** in the supplementary information. The load/bias–time curve for the first mechanical loading cycle is shown in Figure 6b. The domain configuration shown in the first image in Figure 6a was the back-switched configuration after an electrical loading cycle (the same as the last image in Figure 4a). Again, increasing mechanical loading led to the expansion of the a-domain that reached its maximum size under the highest load. After unloading, the a-domain shrank but did not return to its original size and shape, i.e., the size of the c-domain was smaller than that before mechanical loading, which confirms the simulation result in Figure 5 that domain switching was partially reversed.





**Movie 3.** The first mechanical loading-unloading cycle after an electrical loading-unloading cycle



**Movie 4.** The second mechanical loading-unloading cycle after an electrical loading-unloading cycle



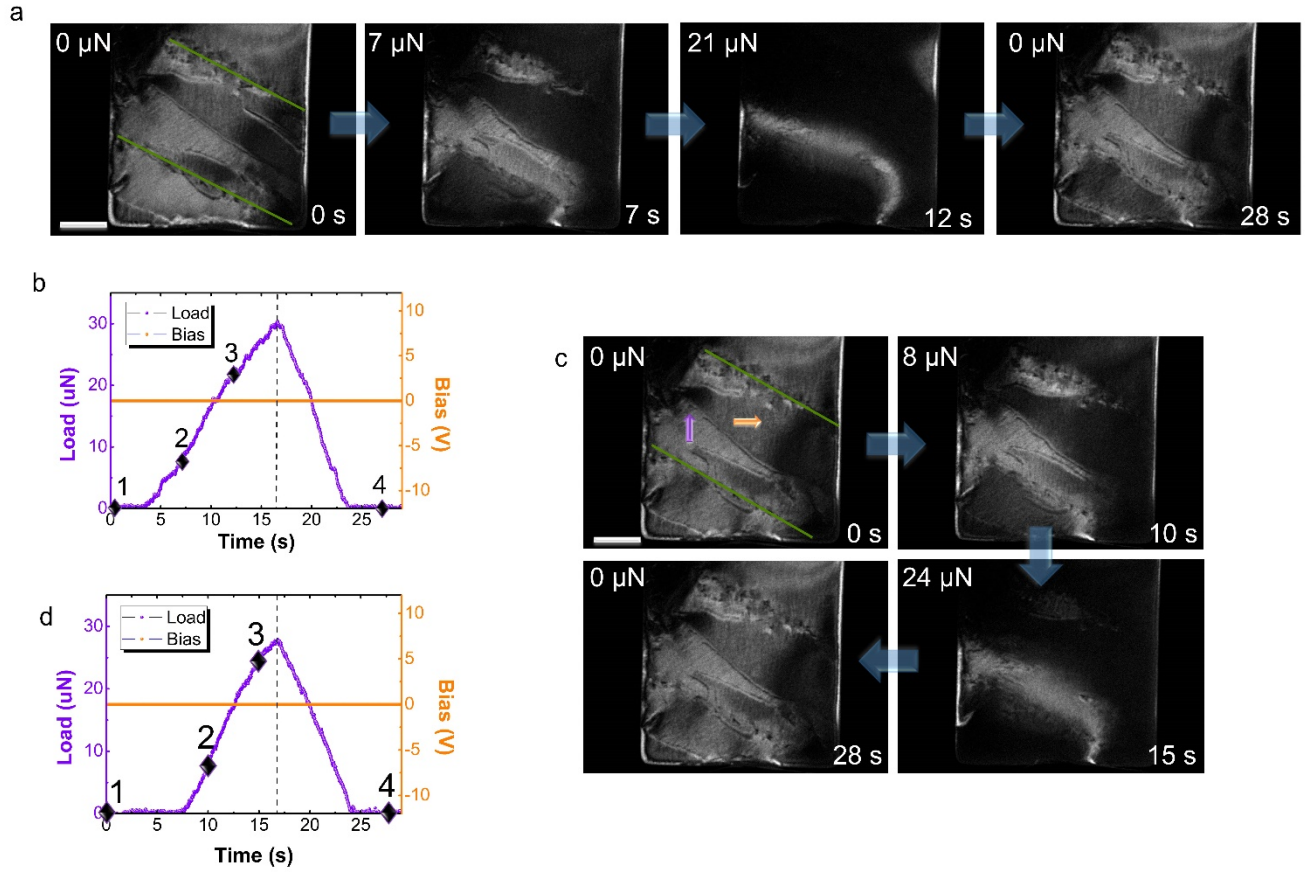


**Figure 6.** Mechanically-reversible and -irreversible ferroelastic domains. A series of images (extracted from the Movie 3 and Movie 4 in the supplementary information) of ferroelastic domains responding to the first mechanical loading–unloading cycle (a) and the second mechanical loading–unloading cycle (c) after an electrical loading cycle. Scale bars, 400 nm. (b) and (d) show the corresponding load/bias–time curves in which the highest load was restricted to  $\sim 28 \mu\text{N}$ .

The effect of mechanical loading for the second and subsequent mechanical loading cycles is shown in Figure 6c and the corresponding load–time curve is presented in Figure 6d. The initial domain configuration (the first image in Figure 6c) is the same as the final domain configuration presented in the last image of Figure 6a. After a complete mechanical loading–unloading cycle, the domain configuration returned to its original structure shown in the first image of Figure 6c, suggesting that the previous mechanically-irreversible state (Figure 6a) has been converted to a mechanically-reversible state after the first mechanical loading–unloading cycle. The two continuous mechanical cycle processes indicate that the reversible nature of ferroelastic domains is repeatable.

### 3. A proposed approach for bit writing and reading

It is now clear that an electrical loading–unloading cycle introduces the mechanically-irreversible state and a subsequent mechanical loading–unloading cycle brings the domain configuration back to the mechanically-reversible state. By taking advantage of the phenomena, an advanced writing and reading approach for non-volatile memories is proposed. In the following discussion, the mechanically-reversible state, i.e.,  $\delta = 0$  in the polarization–stress curve after a mechanical loading–unloading cycle, is defined as the logical signal 0, while the mechanically-irreversible state, i.e.,  $\delta > 0$  after a mechanical loading–unloading cycle, is defined as the logical signal 1.

When domains at the mechanically-reversible state are subjected to a mechanical loading cycle, the mechanically-reversible state remains. This provides the first logical expression:

$$\textit{Reversible state} + \textit{mechanical loading cycle} = \textit{Reversible state}$$

$$0 + \sigma = 0 \quad (1)$$

If the mechanically-reversible state is subjected to an electrical loading cycle, it transfers to the mechanically- irreversible state and this can be expressed by:

$$\textit{Reversible state} + \textit{electrical loading cycle} = \textit{Irreversible state}$$

$$0 + E = 1 \quad (2)$$

When mechanically-irreversible domains experience a mechanical loading cycle, its state switches to the mechanically-reversible one:

$$\textit{Irreversible state} + \textit{mechanical loading cycle} = \textit{Reversible state}$$

$$1 + \sigma = 0 \quad (3)$$

Mechanically-irreversible domains remain after another electrical loading cycle (See the Supplementary Information S1), therefore,

$$\text{Irreversible state} + \text{electrical loading cycle} = \text{Irreversible state}$$

$$1 + E = 1 \quad (4)$$

These four logical expressions provide the fundamental rules for logical identification in writing and reading bits. The ways of writing bits by mechanical and electrical excitations and reading bits by mechanical excitation are illustrated in **Figure 7a**, in which a 4-cell matrix has the original logical states of Aa(1), Ab(1), Ba(0), and Bb(0) (see the first matrix in Figure 7a). Based on the four logical expressions, applying mechanical stress to cells Aa and Ba, and electrical loading to cells Ab and Bb leads to the logical states of Aa(0), Ab(1), Ba(0), and Bb(1), as shown in the second matrix in Figure 7a. Reading the logical states in the four cells is achieved by applying mechanical stress to each of the cells and this process results in the logical state of 0 for all 4 cells, as shown in the third matrix in Figure 7a. Local polarization change ( $\delta$ ) before and after mechanical excitation is used to determine the logical signal of each cell during reading. Aa and Ba follow rule (1) with  $\delta = 0$  while Ab and Bb follow rule (3) with  $\delta \neq 0$ . As has been defined above, it reads 0 if  $\delta = 0$  or 1 if  $\delta \neq 0$  as shown in Figure 7b. Electrical reading can also be achieved when electrical-reversible (the same state as the mechanical-irreversible state) and electrical-irreversible states (the same state as the mechanical-reversible state) are used as two memory states.

While the backswitching drawback can be overcome by using  $\delta=0$  and  $\delta \neq 0$  as the two memory states, the designs of the corresponding reading circuit is not an easy task. A more efficient circuit design is therefore necessary for our proposed bit writing and reading strategy.

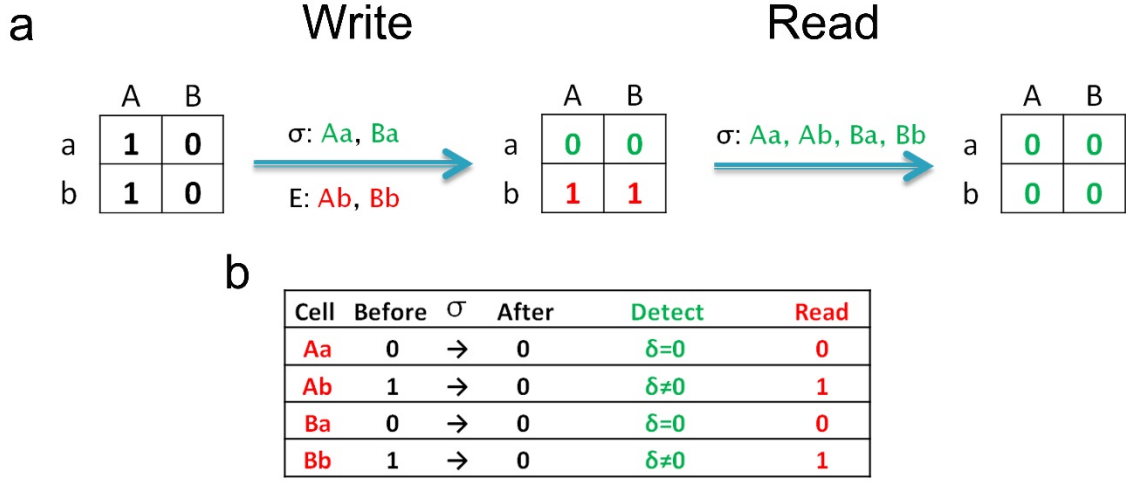


**Figure 7.** Writing and reading bits processes. **(a)** Mechanically-reversible domains are denoted as the logical signal 0 while mechanically-irreversible domains are the logical signal 1. In the writing process, by applying the bias to cells Ab and Bb, and mechanical loading to cells Aa and Ba, the logical states of the 4 cells become Aa(0), Ab(1), Ba(0), and Bb(1), which are independent of their initial states. In the reading process, mechanical loading is applied to the cells and transfers logical states in the cells to the mechanically-reversible state (0). **(b)** By detecting the change of the polarization  $\delta$ , cells are read 0 when  $\delta = 0$  or 1 when  $\delta > 0$ . Cells are therefore read Aa(0), Ab(1), Ba(0), and Bb(1).

#### 4. Conclusions

In conclusion, in-situ TEM experiments and phase-field modelling have been used to explore the combined effects of mechanical stress and electric loading on the ferroelastic domain structures in PMN-33%PT. Results showed that domain structures can be in the mechanically-irreversible state or the mechanically-reversible state depending on if the structures have been subjected to electrical or mechanical excitation. These domain switching behaviours are different from that of normal ferroelectric materials and relaxor-based ferroelectric materials with compositions that are outside MPB. This is due to the low and asymmetric energy barriers among different domains. The two domain reversibility states can be used to represent the logical signals 0 and 1 for non-volatile memories. This logical calculation strategy is not affected by the ferroelastic/ferroelectric domain backswitching and therefore overcome the long-standing problem of backswitching-induced data lose in the memories, significantly enhancing the reliability of the non-volatile memories. Further, the

new writing and reading method allows the use of ferroelastic domains (e.g., the  $90^\circ$  domains in this investigation) and therefore significantly broadens the number of candidate materials for non-volatile memories.

## **Acknowledgements**

The authors are grateful for the scientific and technical support from the Australian Microscopy & Microanalysis Research Facility node at the University of Sydney and the assistance of Dr. David Mitchell of the Electron Microscopy Centre of the University of Wollongong. This research was financially supported by the Australian Research Council. The work at Penn State was supported by the U.S. Department of Energy, Office of Basic Energy Sciences, Division of Materials Sciences and Engineering under Award FG02-07ER46417. This research was supported by the Faculty of Engineering & Information Technologies, The University of Sydney, under the Faculty Research Cluster Program.

## References

- [1] B. H. Park, B. S. Kang, S. D. Bu, T. W. Noh, J. Lee, and W. Jo, *Nature* Lanthanum-substituted bismuth titanate for use in non-volatile memories **401**, 682 (1999).
- [2] S. Das and J. Appenzeller, *Nano Lett.* FETRAM. An Organic Ferroelectric Material Based Novel Random Access Memory Cell **11**, 4003 (2011).
- [3] V. Garcia and M. Bibes, *Nature* ELECTRONICS Inside story of ferroelectric memories **483**, 279 (2012).
- [4] D. Lee, S. M. Yang, T. H. Kim, B. C. Jeon, Y. S. Kim, J. G. Yoon, H. N. Lee, S. H. Baek, C. B. Eom, and T. W. Noh, *Adv. Mater.* Multilevel Data Storage Memory Using Deterministic Polarization Control **24**, 402 (2012).
- [5] H. Lu, C. W. Bark, D. E. de los Ojos, J. Alcala, C. B. Eom, G. Catalan, and A. Gruverman, *Science* Mechanical Writing of Ferroelectric Polarization **336**, 59 (2012).
- [6] R. Guo, L. You, Y. Zhou, Z. S. Lim, X. Zou, L. Chen, R. Ramesh, and J. L. Wang, *Nat. Commun.* Non-volatile memory based on the ferroelectric photovoltaic effect **4**, 1990 (2013).
- [7] Z. Chen, X. Wang, S. Ringer, and X. Liao, *Phys. Rev. Lett.* Manipulation of Nanoscale Domain Switching Using an Electron Beam with Omnidirectional Electric Field Distribution **117**, 027601 (2016).
- [8] P. Gao, C. T. Nelson, J. R. Jokisaari, Y. Zhang, S. H. Baek, C. W. Bark, E. Wang, Y. M. Liu, J. Y. Li, C. B. Eom, and X. Q. Pan, *Adv. Mater.* Direct Observations of Retention Failure in Ferroelectric Memories **24**, 1106 (2012).
- [9] D. J. Kim, J. Y. Jo, Y. S. Kim, Y. J. Chang, J. S. Lee, J. G. Yoon, T. K. Song, and T. W. Noh, *Phys. Rev. Lett.* Polarization relaxation induced by a depolarization field in ultrathin ferroelectric BaTiO<sub>3</sub> capacitors **95**, 237602 (2005).
- [10] O. Lohse, M. Grossmann, U. Boettger, D. Bolten, and R. Waser, *J. Appl. Phys.* Relaxation mechanism of ferroelectric switching in Pb(Zr,Ti)O<sub>3</sub> thin films **89**, 2332 (2001).
- [11] J. Glaum, T. Granzow, and J. Rodel, *J. Appl. Phys.* Evaluation of domain wall motion in bipolar fatigued lead-zirconate-titanate: A study on reversible and irreversible contributions **107**, 104119 (2010).
- [12] J. H. Li, P. T. Lin, and B. W. Wessels, *J. Appl. Phys.* Polarization reversal and backswitching dynamics in epitaxial BaTiO<sub>3</sub> thin films **106**, 054113 (2009).
- [13] I. Vrejoiu, G. Le Rhun, N. D. Zakharov, D. Hesse, L. Pintilie, and M. Alexe, *Philos. Mag.* Threading dislocations in epitaxial ferroelectric PbZr<sub>0.2</sub>Ti<sub>0.8</sub>O<sub>3</sub> films and their effect on polarization backswitching **86**, 4477 (2006).
- [14] X. J. Lou and J. Wang, *J. Appl. Phys.* Bipolar and unipolar electrical fatigue in ferroelectric lead zirconate titanate thin films: An experimental comparison study **108**, 034104 (2010).
- [15] X. Z. Chen, Q. Li, X. Chen, X. Guo, H. X. Ge, Y. Liu, and Q. D. Shen, *Adv. Funct. Mater.* Nano-Imprinted Ferroelectric Polymer Nanodot Arrays for High Density Data Storage **23**, 3124 (2013).
- [16] S. H. Baek, H. W. Jang, C. M. Folkman, Y. L. Li, B. Winchester, J. X. Zhang, Q. He, Y. H. Chu, C. T. Nelson, M. S. Rzchowski, X. Q. Pan, R. Ramesh, L. Q. Chen, and C. B. Eom, *Nat. Mater.* Ferroelastic switching for nanoscale non-volatile magnetoelectric devices **9**, 309 (2010).
- [17] A. I. Khan, X. Marti, C. Serrao, R. Ramesh, and S. Salahuddin, *Nano Lett.* Voltage-Controlled Ferroelastic Switching in Pb(Zr<sub>0.2</sub>Ti<sub>0.8</sub>)O<sub>3</sub> Thin Films **15**, 2229 (2015).

- [18] M. P. Cruz, Y. H. Chu, J. X. Zhang, P. L. Yang, F. Zavaliche, Q. He, P. Shafer, L. Q. Chen, and R. Ramesh, *Phys. Rev. Lett.* Strain control of domain-wall stability in epitaxial BiFeO<sub>3</sub> (110) films **99**, 217601 (2007).
- [19] W. J. Chen, Y. Zheng, W. M. Xiong, X. Feng, B. Wang, and Y. Wang, *Sci Rep* Effect of Mechanical Loads on Stability of Nanodomains in Ferroelectric Ultrathin Films: Towards Flexible Erasing of the Non-Volatile Memories **4**, 5339 (2014).
- [20] Z. B. Chen, L. Hong, F. F. Wang, S. P. Ringer, L. Q. Chen, H. S. Luo, and X. Z. Liao, *Phys. Rev. Lett.* Facilitation of Ferroelectric Switching via Mechanical Manipulation of Hierarchical Nanoscale Domain Structures **118**, 017601 (2017).
- [21] G. Catalan, L. J. Sinnamon, and J. M. Gregg, *J. Phys.-Condes. Matter* The effect of flexoelectricity on the dielectric properties of inhomogeneously strained ferroelectric thin films **16**, 2253 (2004).
- [22] M. S. Majdoub, P. Sharma, and T. Cagin, *Phys. Rev. B* Enhanced size-dependent piezoelectricity and elasticity in nanostructures due to the flexoelectric effect **77**, 125424 (2008).
- [23] S. E. Park and T. R. Shrout, *J. Appl. Phys.* Ultrahigh strain and piezoelectric behavior in relaxor based ferroelectric single crystals **82**, 1804 (1997).
- [24] Y. M. Jin, Y. U. Wang, A. G. Khachaturyan, J. F. Li, and D. Viehland, *Phys. Rev. Lett.* Conformal miniaturization of domains with low domain-wall energy: Monoclinic ferroelectric states near the morphotropic phase boundaries **91**, 197601 (2003).
- [25] Y. Sato, T. Hirayama, and Y. Ikuhara, *Phys. Rev. Lett.* Real-Time Direct Observations of Polarization Reversal in a Piezoelectric Crystal: Pb(Mg<sub>1/3</sub>Nb<sub>2/3</sub>)O<sub>3</sub>-PbTiO<sub>3</sub> Studied via In Situ Electrical Biasing Transmission Electron Microscopy **107**, 187601 (2011).
- [26] M. Marsilius, J. Frederick, W. Hu, X. L. Tan, T. Granzow, and P. D. Han, *Adv. Funct. Mater.* Mechanical Confinement: An Effective Way of Tuning Properties of Piezoelectric Crystals **22**, 797 (2012).
- [27] Q. Wan, C. Chen, and Y. P. Shen, *J. Appl. Phys.* Effects of stress and electric field on the electromechanical properties of Pb(Mg<sub>1/3</sub>Nb<sub>2/3</sub>)O<sub>3</sub>-0.32PbTiO<sub>3</sub> single crystals **98**, 024103 (2005).
- [28] M. G. Han, Y. M. Zhu, L. J. Wu, T. Aoki, V. Volkov, X. Y. Wang, S. C. Chae, Y. S. Oh, and S. W. Cheong, *Adv. Mater.* Ferroelectric Switching Dynamics of Topological Vortex Domains in a Hexagonal Manganite **25**, 2415 (2013).
- [29] Y. Sato, T. Hirayama, and Y. Ikuhara, *Appl. Phys. Lett.* Evolution of nanodomains under DC electrical bias in Pb(Mg<sub>1/3</sub>Nb<sub>2/3</sub>)O<sub>3</sub>-PbTiO<sub>3</sub>: An In-situ transmission electron microscopy study **100**, 172902 (2012).
- [30] L. Q. Chen, *Ann. Rev. Mater. Res.* Phase-field models for microstructure evolution **32**, 113 (2002).
- [31] G. S. Xu, H. S. Luo, H. Q. Xu, and Z. W. Yin, *Phys. Rev. B* Third ferroelectric phase in PMNT single crystals near the morphotropic phase boundary composition **64**, 020102 (2001).
- [32] A. K. Singh, D. Pandey, and O. Zaharko, *Phys. Rev. B* Powder neutron diffraction study of phase transitions in and a phase diagram of (1-x) Pb(Mg<sub>1/3</sub>Nb<sub>2/3</sub>)O<sub>3</sub>-xPbTiO<sub>3</sub> **74**, 024101 (2006).
- [33] D. Viehland, *J. Appl. Phys.* Symmetry-adaptive ferroelectric mesostates in oriented Pb(Bi<sub>1/3</sub>Bi<sub>2/3</sub>)O<sub>3</sub>-PbTiO<sub>3</sub> crystals **88**, 4794 (2000).
- [34] S. Bhattacharyya, J. R. Jinschek, H. Cao, Y. U. Wang, J. F. Li, and D. Viehland, *Appl. Phys. Lett.* Direct high-resolution transmission electron microscopy observation of tetragonal nanotwins within the monoclinic M(C) phase of Pb(Mg(1/3)Nb(2/3))O<sub>3</sub>-0.35PbTiO<sub>3</sub> crystals **92**, 142904 (2008).



- [35] H. Wang, J. Zhu, N. Lu, A. A. Bokov, Z. G. Ye, and X. W. Zhang, *Appl. Phys. Lett.* Hierarchical micro-/nanoscale domain structure in M-C phase of (1-x)Pb(Mg<sub>1/3</sub>Nb<sub>2/3</sub>)O-3-xPbTiO(3) single crystal **89**, 042908 (2006).
- [36] Y. Nahas, S. Prokhorenko, I. Kornev, and L. Bellaiche, *Phys. Rev. Lett.* Topological Point Defects in Relaxor Ferroelectrics **116**, 127601 (2016).
- [37] P. Paruch and J. Guyonnet, *Comptes Rendus Physique* Nanoscale studies of ferroelectric domain walls as pinned elastic interfaces **14**, 667 (2013).
- [38] F. Chu, I. M. Reaney, and N. Setter, *J. Am. Ceram. Soc.* ROLE OF DEFECTS IN THE FERROELECTRIC RELAXER LEAD SCANDIUM TANTALATE **78**, 1947 (1995).
- [39] C. L. Jia, V. Nagarajan, J. Q. He, L. Houben, T. Zhao, R. Ramesh, K. Urban, and R. Waser, *Nat. Mater.* Unit-cell scale mapping of ferroelectricity and tetragonality in epitaxial ultrathin ferroelectric films **6**, 64 (2007).
- [40] P. Gao, J. Britson, J. R. Jokisaari, C. T. Nelson, S. H. Baek, Y. R. Wang, C. B. Eom, L. Q. Chen, and X. Q. Pan, *Nat. Commun.* Atomic-scale mechanisms of ferroelastic domain-wall-mediated ferroelectric switching **4**, 2791 (2013).
- [41] See Supplemental Material [url], which includes Refs. [42-56].
- [42] H. S. Luo, G. S. Xu, H. Q. Xu, P. C. Wang, and Z. W. Yin, *Jpn. J. Appl. Phys. Part 1 - Regul. Pap. Short Notes Rev. Pap.* Compositional homogeneity and electrical properties of lead magnesium niobate titanate single crystals grown by a modified Bridgman technique **39**, 5581 (2000).
- [43] Y. L. Li, S. Y. Hu, Z. K. Liu, and L. Q. Chen, *Acta Materialia* Effect of substrate constraint on the stability and evolution of ferroelectric domain structures in thin films **50**, 395 (2002).
- [44] Y. M. M. Jin, Y. U. Wang, and A. G. Khachaturyan, *Philos. Mag.* Three-dimensional phase field microelasticity theory of a multivoid multicroack system in an elastically anisotropic body: model and computer simulations **83**, 1587 (2003).
- [45] Khachaturyan, A. G. and G. A. Shatalov, *Soviet Physics JETP-USSR* THEORY OF MACROSCOPIC PERIODICITY FOR A PHASE TRANSITION IN SOLID STATE **29**, 557 (1969).
- [46] R. Zhang, B. Jiang, and W. W. Cao, *Appl. Phys. Lett.* Single-domain properties of 0.67Pb(Mg<sub>1/3</sub>Nb<sub>2/3</sub>)O-3-0.33PbTiO(3) single crystals under electric field bias **82**, 787 (2003).
- [47] Y. Lu, D. Y. Jeong, Z. Y. Cheng, Q. M. Zhang, H. S. Luo, Z. W. Yin, and D. Viehland, *Appl. Phys. Lett.* Phase transitional behavior and piezoelectric properties of the orthorhombic phase of Pb(Mg(1/3)Nb(2/3))O(3)-PbTiO(3) single crystals **78**, 3109 (2001).
- [48] Y. L. Li, S. Y. Hu, Z. K. Liu, and L. Q. Chen, *Appl. Phys. Lett.* Effect of electrical boundary conditions on ferroelectric domain structures in thin films **81**, 427 (2002).
- [49] Y. L. Li, L. Q. Chen, G. Asayama, D. G. Schlom, M. A. Zurbuchen, and S. K. Streiffer, *J. Appl. Phys.* Ferroelectric domain structures in SrBi<sub>2</sub>Nb<sub>2</sub>O<sub>9</sub> epitaxial thin films: Electron microscopy and phase-field simulations **95**, 6332 (2004).
- [50] L. Q. Chen and J. Shen, *Comput. Phys. Commun.* Applications of semi-implicit Fourier-spectral method to phase field equations **108**, 147 (1998).
- [51] R. J. Xu, S. Liu, I. Grinberg, J. Karthik, A. R. Damodaran, A. M. Rappe, and L. W. Martin, *Nat. Mater.* Ferroelectric polarization reversal via successive ferroelastic transitions **14**, 79 (2015).
- [52] S. Choudhury, L. Q. Chen, and Y. L. Li, *Appl. Phys. Lett.* Correlation between number of ferroelectric variants and coercive field of lead zirconate titanate single crystals **91**, 032902 (2007).
- [53] P. K. Larsen, R. Cuppens, and G. Spierings, *Ferroelectrics* FERROELECTRIC MEMORIES **128**, 265 (1992).

- [54] S. Zhang, J. Luo, F. Li, R. J. Meyer Jr, W. Hackenberger, and T. R. ShROUT, *Acta Materialia* Polarization fatigue in  $\text{Pb}(\text{In}_{0.5}\text{Nb}_{0.5})\text{O}_3\text{--Pb}(\text{Mg}_{1/3}\text{Nb}_{2/3})\text{O}_3\text{--PbTiO}_3$  single crystals **58**, 3773 (2010).
- [55] K. Takemura, M. Ozgul, V. Bornand, S. Trolier-McKinstry, and C. A. Randall, *J. Appl. Phys.* Fatigue anisotropy in single crystal  $\text{Pb}(\text{Zn}_{1/3}\text{Nb}_{2/3})\text{O}_3\text{--PbTiO}_3$  **88**, 7272 (2000).
- [56] E. W. Sun and W. W. Cao, *Prog. Mater. Sci.* Relaxor-based ferroelectric single crystals: Growth, domain engineering, characterization and applications **65**, 124 (2014).
- [57] V. V. Shvartsman and A. L. Kholkin, *Phys. Rev. B* Domain structure of  $0.8\text{Pb}(\text{Mg}_{1/3}\text{Nb}_{2/3})\text{O}_3\text{--}0.2\text{PbTiO}_3$  studied by piezoresponse force microscopy **69**, 014102 (2004).
- [58] M. D. Glinchuk, *British Ceramic Transactions* Relaxor ferroelectrics: from cross superparaelectric model to random field theory **103**, 76 (2004).
- [59] F. Li, S. Zhang, T. Yang, Z. Xu, N. Zhang, G. Liu, J. Wang, J. Wang, Z. Cheng, Z.-G. Ye, J. Luo, T. R. ShROUT, and L.-Q. Chen, *Nat. Commun.* The origin of ultrahigh piezoelectricity in relaxor-ferroelectric solid solution crystals **7**, 13807 (2016).
- [60] V. V. Shvartsman, B. Dkhil, and A. L. Kholkin, in *Annual Review of Materials Research, Vol 43*, edited by D. R. Clarke (Annual Reviews, Palo Alto, 2013), pp. 423.
- [61] P. Gao, J. Britson, C. T. Nelson, J. R. Jokisaari, C. Duan, M. Trassin, S. H. Baek, H. Guo, L. Z. Li, Y. R. Wang, Y. H. Chu, A. M. Minor, C. B. Eom, R. Ramesh, L. Q. Chen, and X. Q. Pan, *Nat. Commun.* Ferroelastic domain switching dynamics under electrical and mechanical excitations **5**, 3801 (2014).
- [62] Y. Gaillard, A. H. Macias, J. Munoz-Saldana, M. Anglada, and G. Trapaga, *J. Phys. D-Appl. Phys.* Nanoindentation of  $\text{BaTiO}_3$ : dislocation nucleation and mechanical twinning **42**, 085502 (2009).
- [63] R. C. Smith and C. L. Hom, *J. Intell. Mater. Syst. Struct.* Domain wall theory for ferroelectric hysteresis **10**, 195 (1999).
- [64] I. W. Chen and Y. Wang, *Ferroelectrics* A domain wall model for relaxor ferroelectrics **206**, 245 (1998).
- [65] X. B. Ren, *Nat. Mater.* Large electric-field-induced strain in ferroelectric crystals by point-defect-mediated reversible domain switching **3**, 91 (2004).
- [66] F. Li, L. Jin, Z. Xu, and S. Zhang, *Applied Physics Reviews* Electrostrictive effect in ferroelectrics: An alternative approach to improve piezoelectricity **1**, 011103 (2014).
- [67] J. Wang, S. Q. Shi, L. Q. Chen, Y. L. Li, and T. Y. Zhang, *Acta Materialia* Phase field simulations of ferroelectric/ferroelastic polarization switching **52**, 749 (2004).